Earth and Planetary Science Letters 402 (2014) 82–89

Contents lists available at ScienceDirect

Earth and Planetary Science Letters

www.elsevier.com/locate/epsl

# A sharp cratonic lithosphere–asthenosphere boundary beneath the American Midwest and its relation to mantle flow

K. Foster, K. Dueker *, B. Schmandt, H. Yuan

ARTICLE INFO

*Article history:*
Accepted 12 November 2013
Available online 12 December 2013
Editor: P. Shearer

*Keywords:*
lithosphere–asthenosphere boundary
cratonic lithosphere
mid-lithosphere discontinuity
receiver functions
teleseismic converted waves

ABSTRACT

Beneath the American Midwest, S-to-P (Sp) converted wave imaging and multi-mode surface wave tomography identify a north-trending transition in seismic structure at 150–250 km depth. To the east of this American Midwest transition (AMT), the lithosphere–asthenosphere boundary (LAB) is imaged as a 1–2% Sp/Sv amplitude arrival at 200–240 km depth, consistent with the depth of negative shear velocity and azimuthal anisotropy gradients imaged by surface wave tomography. To the west of the AMT, Sp conversions are much shallower at 150–190 km depth and are much weaker (<0.7%) or absent. Azimuthal anisotropy constrained by surface wave tomography also changes across the AMT, with stronger anisotropy to the east of the transition beneath the thicker lithospheric root. We suggest that the seismic changes across the AMT can be explained by considering the effects of asthenospheric flow beneath the leading edge of the thick lithospheric root. The mantle flow is dominantly driven by the drift of the North America plate. Locally higher flow velocities are expected where the asthenosphere is forced to flow beneath the thicker root. This mantle underflow could create a sharper seismic LAB east of the AMT via two effects. First, the local increase in flow velocities could steepen the thermal gradient at the base of the lithosphere, and hence the isotropic velocity contrast. Second, the increased strain rate along edge of the lithosphere could enhance the magnitude of azimuthal anisotropy. Our results suggest that seismically detectable LAB sharpness variations could be used to constrain geographic variations in coupling between plates and mantle convection. A secondary result is the image of a Mid-Lithospheric Discontinuity arrival at 80–110 km depth that is found primarily to the east of the AMT. This arrival is interpreted as produced by a layer of low-velocity metasomatic minerals that have accumulated since the >1.8 Ga creation of the lithosphere.

© 2013 Elsevier B.V. All rights reserved.

## 1. Introduction

The magnitude of stress coupling between mantle convection and the base of the plates is a first-order issue in assessing the force balances on plates, and hence the motion of the plate mosaic (Forsyth and Uyeda, 1975; Ghosh et al., 2013). A first-order control with regard to the coupling between tectonic plates and underlying mantle convection is the physical state property variations at the base of the lithosphere that produce a viscosity gradient that has a 2–3 order of magnitude decrease across the 1000–1300 °C thermal gradient (Sleep, 2011). This basal viscosity gradient is where the buoyantly driven flow of the mantle (Ghosh and Holt, 2012) and the relative motion of the plate must be accommodated via exchange of stress.

Generally increasing viscosity with depth predicts that the rheologically mobile boundary layer in the ~1000–1300 °C interval will experience higher flow stresses as lithospheric thickness increases, potentially producing an approximately 250 km limit on lithospheric thickness for the present day convective regime (Cooper and Conrad, 2009). Additionally, mantle flow around undulations in lithospheric thickness and variations in relative velocity between the lithosphere and asthenosphere will modulate the shear strain rates in the basal thermal boundary layer that is capable of deforming viscously. Such flow induced shear strain variations could create variations in the strength of olivine LPO development that would be observed as velocity anisotropy detectable with seismology (Kaminski and Ribe, 2002; Ribe, 1989). Thus, seismic interrogation of physical property variations at the base of the lithosphere can help to constrain geographic variations in the degree of plate–mantle stress coupling.

Ideally, one seeks to seismically interrogate a region where a plate's basal physical properties are changing. Here we focus on such a region in the American Midwest, where the lithosphere thickens substantially and the North American plate motion is nearly perpendicular to the strike of the narrow area over which the lithosphere thickens. In this scenario, the sub-lithospheric

* Corresponding author.
*E-mail address:* dueker@uwyo.edu (K. Dueker).

0012-821X/$ – see front matter © 2013 Elsevier B.V. All rights reserved.
http://dx.doi.org/10.1016/j.epsl.2013.11.018

mantle must flow down and below the thickened lithospheric root and hence the mantle flow must accelerate based on Bernoulli's principle given the reasonable assumption that the base of the low viscosity asthenospheric channel remains relatively constant.

In thin lithosphere areas (<130 km), the LAB velocity gradient can be adequately resolved via inversion of fundamental mode surface wave dispersion data (Lebedev et al., 2009; Pedersen et al., 2009). However, in thick lithosphere areas (>130 km), fundamental mode resolution at these depths is poor and higher-mode surface wave data is required to constrain velocity gradients associated with the base of the lithosphere (Yuan and Romanowicz, 2010). Even higher resolution of velocity gradients at the base of the plates is provided by Ps and Sp converted wave images that directly sense velocity gradients (Farra and Vinnik, 2000; Rychert et al., 2007) and do not require a regularized inversion to image structure. In thin lithosphere areas, Ps converted waves can isolate LAB arrivals with minimal interference with free-surface to Moho reverberations (Rychert et al., 2005). However, in thick lithosphere areas, Ps prospecting for LAB arrivals is problematic due to the overprinting of small amplitude LAB arrivals by free-surface to Moho reverberations (Julià, 2007).

A remedy with regard to this Ps Moho reverberation interference is the use of converted Sp waves that has proven useful for imaging thick lithosphere LAB arrivals because Sp converted arrivals are not overprinted by Moho reverberations (Farra and Vinnik, 2000). The caveat to this advantage over Ps receiver functions is that S-wave receiver functions have reduced imaging power due to: less high-frequency bandwidth, fewer usable earthquake recordings due to epicentral distance range constraints, deconvolutional issues associated with the S and SKS branch cross-over at 84° (Yuan et al., 2006a), and, the requirement that SV polarized incident S-waves be used. Herein, a comparison of Sp and multi-mode surface wave images is performed to constrain lateral variations in isotropic and anisotropic seismic structure across the edge of North America's cratonic core in the American upper Midwest.

## 2. Data and methods

All EarthScope USArray seismic data recorded through November 2011 and most of the available PASSCAL broad-band data were processed into an Sp image that extends from the west coast to the longitude of Chicago with 41,731 binned Sp receiver functions. From this dataset, a subset within the American Midwest sampled by 6993 receiver functions is presented (Fig. 1). Our Sp receiver functions dataset consists of both the direct S-wave branch from 58°–84° epicentral distance and the SKS branch from 84°–110° epicentral distance. The percentage of direct-Sp and SKSp arrivals in our dataset is 64% and 36% respectively. Images made using only SKSp arrivals are noisy because the data sampling is reduced to 36% of the full dataset. With regard to P contamination of SKSp arrivals, we note that only pPPPP arrivals from >300 km depth event arrivals are predicted to arrive in our uppermost mantle time window of interest. Thus, given the rarity of this occurrence, we are not concerned about P-phase contamination of our SKSp dataset. To minimize cross-contamination between the SKS and S branches, extensive data culling and careful time windowing of the first-arriving S-wave packet was performed. The data culling consists of viewing up to 440 USArray three-component traces on multi-monitors and interactively processing the data. The first S-wave packet is windowed with an 8–12 s window and the SV-component relative travel-time residuals are measured and applied to line up the data so that waveform coherence may be assessed. Traces that are incoherent are deleted and events that have significant variations in the first-arriving S-wave packet waveshape are not used as that would violate our common source wavelet assumption in our deconvolution method. Rather than deconvolving the entire SV-component traces from the P-component traces, the first-S arrival is windowed and used in our source estimation procedure (Hansen and Dueker, 2009).

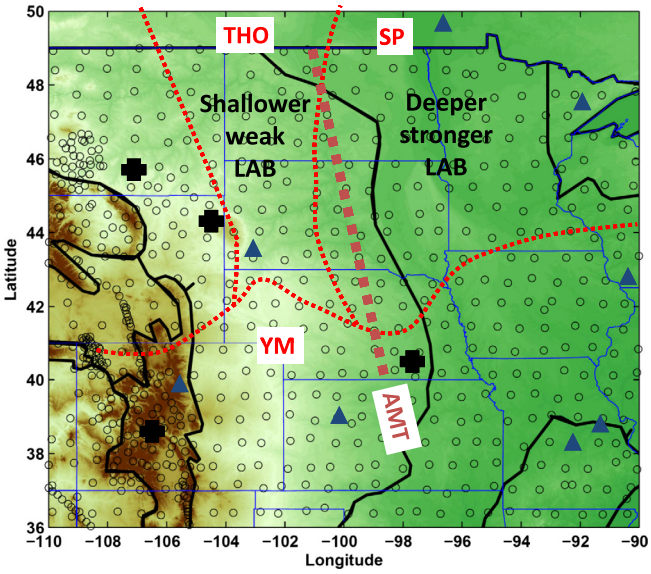


**Fig. 1.** Stations, topography, crustal province boundaries. The boundary between a deeper LAB and shallower weak to absent LAB signals is demarked as the American Midwest Transition (AMT) red dotted line. The crustal provinces boundaries are outlined as red dotted lines: circa. 2.6 Ga Superior Province (SP); 1.8–1.9 Ga Trans-Hudson orogen (THO); 1.8–1.6 Ga Yavapai–Mazatzal (YM). The black crosses show carbonatite intrusions locations that are consistent with the re-melting of an ancient metasomatic layer. The blue triangles are the permanent stations analyzed by Abt et al. (2010) discussed in text.

Our method to produce receiver functions (Hansen and Dueker, 2009) is significantly different with respect to signal station spectral deconvolution methods (Langston, 1977; Vinnik, 1977) that use the incident component as an estimate of the source wavelet. Instead, we assume for each event that a common source wavelet is incident at all stations (up to 440) and a least-square inverse is conducted to isolate the source wavelet spectra from the three-component receiver function spectra. Additionally, we do not assume that pure mode scattering (Sv–Sv) potential is zero as done in traditional receiver function analysis. The receiver function phase spectra are calculated by using the assumption that pure-mode scattering (SV to SV in this work) is effectively minimum phase for velocity models relevant to the Earth (Bostock, 2004) and the Kolmogorov minimum phase operator (Kolmogorov, 1939) is used in the phase reconstruction of the receiver functions (Mercier et al., 2006).

The Sp receiver function data were filtered using a suite of filter band-pass values and migrated into our image volume using a common-conversion point migration method (Dueker and Sheehan, 1997). The band-passes used were a high pass of 30 s with low-passes of 2 s, 3 s, 4 s, 6 s, and 8 s. The image volume is parameterized using 110 km wide image bins that are two km thick. In the upper 150 km, our migration velocity model consists of an isotropic shear velocity model (Shen et al., 2013) that is smoothly merged with the AK135 velocity model at 150–170 km depth to produce a model that extends to 300 km depth. A corresponding P-wave velocity model is derived by scaling this shear velocity model to a P-wave model using an assumed crust and mantle $V_p/V_s$ of 1.76 and 1.81 respectively. Sp times are mapped to depth by extracting the S- and P-wave velocity functions along the incident and converted ray-paths and using these velocity functions in the one-dimensional Sp move out equation.

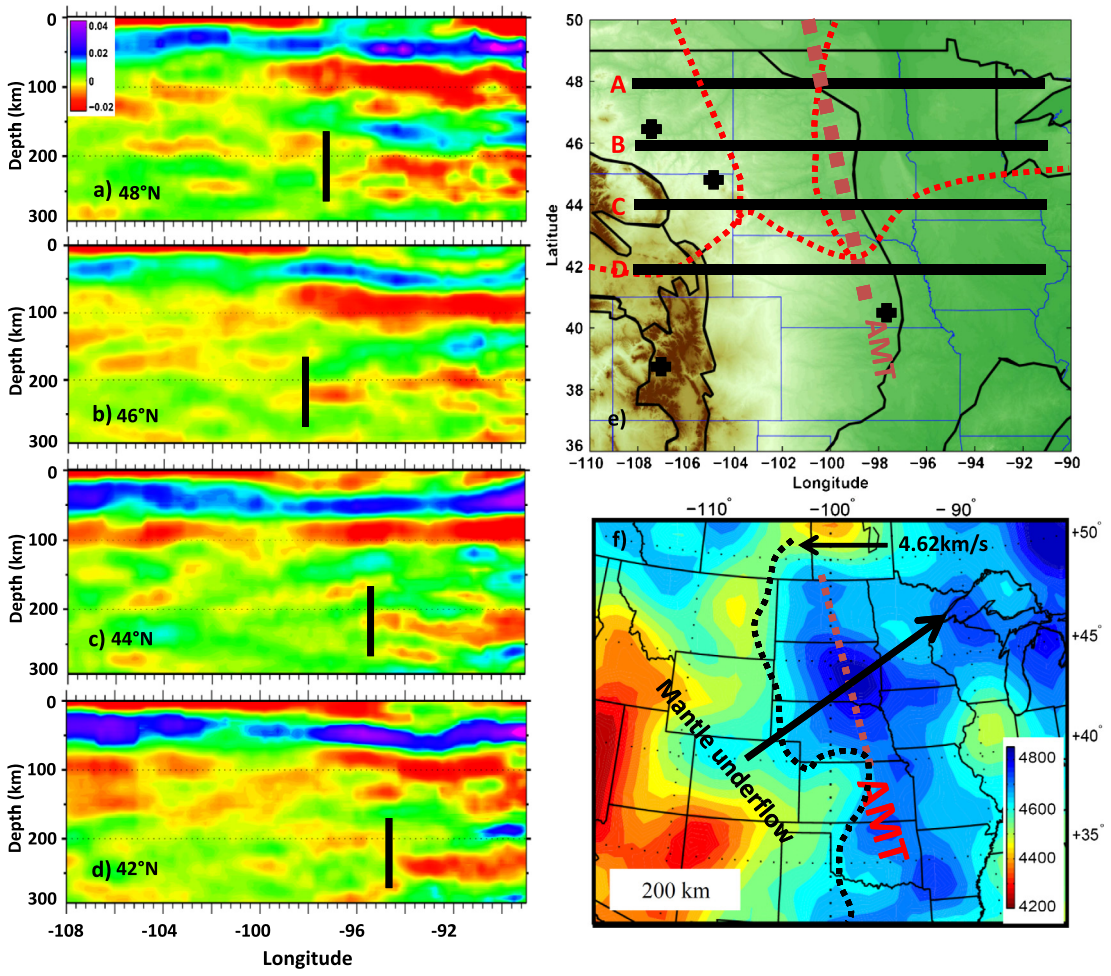


**Fig. 2.** Seismic structure in American upper Midwest. (a)–(d) E–W Sp sections at indicated latitudes with short black line indicate edge of 1–2% Sp/Sv LAB arrival at 200–240 km depth. (e) Cross-sections, crustal province boundaries, and American Midwest transition (AMT). (f) Isotropic velocity at 200 km depth from Yuan and Romanowicz (2010). The 4.62 km/s at 150 km depth (Fig. 4(d)) is show as black dotted line. The approximate dip of the lithosphere using the 4.80 km/s contour at 200 km depth line is 14–26°. The mantle underflow arrow is based on the North American absolute plate motion and the high stress tractions (2.1 MPa) found by convection modeling of Ghosh et al. (2013).

The tomographic velocity model we compare our Sp image to is derived from waveform fitting of long-period fundamental and higher-mode seismograms constrained by SKS shear-wave measurements to provide isotropic and radial and azimuthal anisotropy images (Yuan and Romanowicz, 2010). The model used herein is derived from permanent and USArray recordings through the end of 2011 (Yuan et al., 2011). The use of higher-mode seismic energy and the SKS measurements is important to provide images of isotropic and anisotropic velocity variations at 180–250 km depths where Sp signals are imaged. We refer to this velocity model in our text as Yuan and Romanowicz (2010).

## 3. Results

### 3.1. LAB sharpness and depth across the AMT

E–W Sp cross-sections through the American upper Midwest find an LAB arrival at 200–240 km depth to the east of a north striking boundary at 98–95°W longitude, but not to the west of this boundary (Fig. 2(a)–(d)). The color palette used to render Fig. 2(a)–(d) is designed to highlight the weak negative velocity gradient arrivals and a more symmetric color palette is shown in Supp. Fig. 1. We term this transition the American Midwest Transition (AMT). Correspondingly, our N–S cross-sections show this difference in LAB arrivals across the AMT with <0.7% arrivals at 150–190 km depth west of the AMT and 0.7%–2% amplitude Sp arrivals at 200–240 km depth to the east of the AMT (Fig. 3(a)–(b)). The AMT demarks a thickening of the lithosphere to the east of the AMT based on the deepening of the 4.62 km/s isotropic velocity contour to the east (Figs. 2(f), 3(d), Supp. Fig. 2). Using these velocity contours, the estimated dip of the lithospheric thickening to the east is 14–26°.

Another important seismic variation to the east of the AMT is the higher azimuthal anisotropy strength at 250 km depth from Yuan and Romanowicz (2010) (Fig. 3(e)). At this depth, the orientation of the azimuthal anisotropy is N60°W that is very close to the absolute North American plate drift direction. Thus, this azimuthal anisotropy is interpreted as manifesting plate shear in the asthenosphere. Comparison of the east of AMT area where the cratonic LAB is observed with the Yuan and Romanowicz (2010) velocity model finds a shear velocity decrement of ~4% along with an increase in azimuthal anisotropy strength (Figs. 3(e), 4(b), (c), Supp. Figs. 3, 4). Thus, we interpret the seismic origin of our LAB arrivals as manifesting gradients in both the isotropic velocity and a 50–100% increase in azimuthal anisotropy strength in the asthenosphere that is oriented parallel to plate motion (Fig. 3(e), Supp. Figs. 3, 4). Inspection of the imaged LAB arrival shows that it is often composed of two arrivals that are shingled. However, at present whether this shingled structure is resolved or just image noise

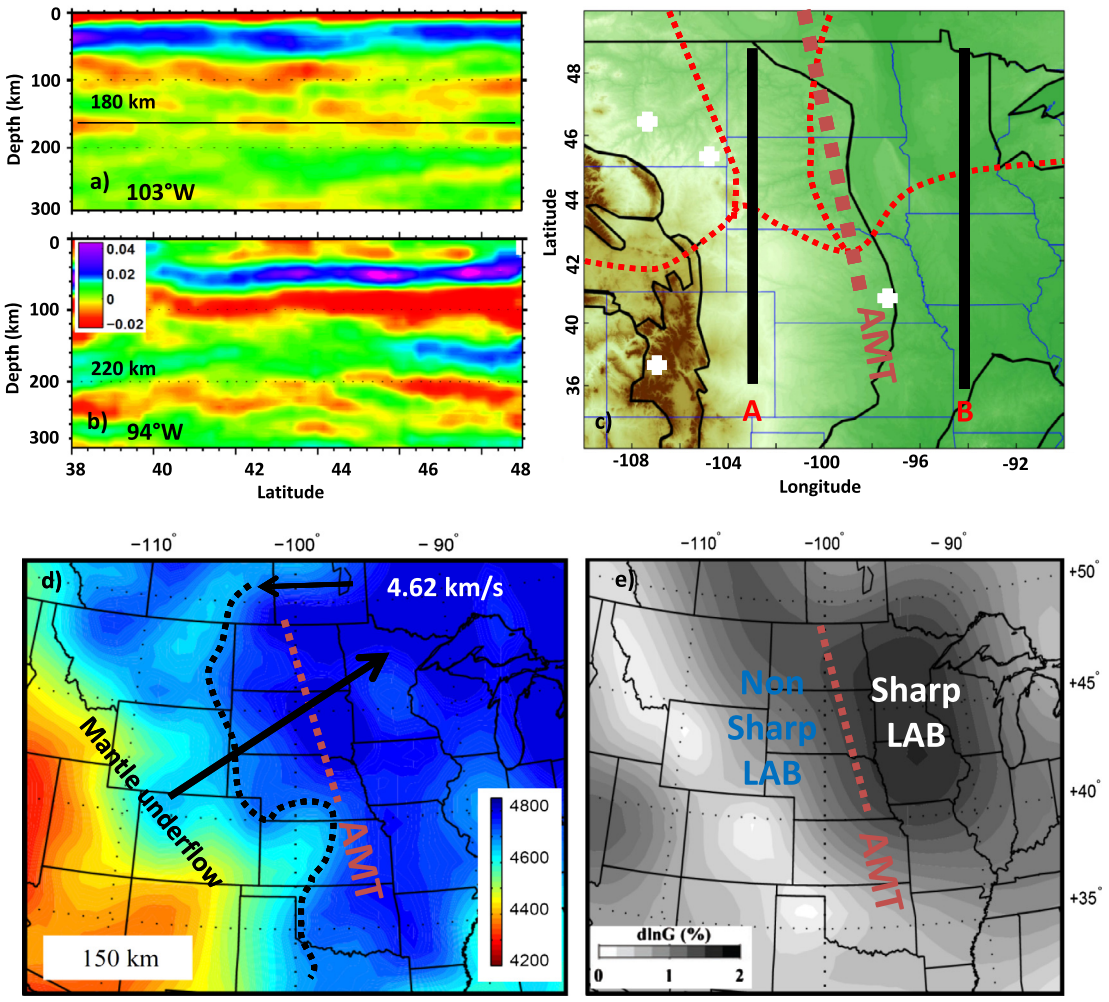


**Fig. 3.** Seismic structure in American upper Midwest. (a)–(b) N–S Sp sections at indicated longitudes. (c) Sp section locations. The American Midwest Transition (AMT) is demarked as red dotted line. See Fig. 1 for other annotation definitions. (d) Isotropic velocity at 150 km depth from Yuan and Romanowicz (2010). (e) Azimuthal anisotropy strength at 250 km from Yuan and Romanowicz (2010). The LAB signal east of the AMT is demarked as the dotted red line that we interpret in text as shear strain localization related to mantle flow under the thickened lithosphere (Fig. 2(f)).

remains equivocal. Noteworthy is that the LAB arrival amplitudes are small (0.7–2% Sp/SV amplitude) because velocity gradients are generally expected to be broad at the base of a thick lithosphere (e.g., Abt et al., 2010). Additionally, the signal to noise ratio in the image volume could use improvement as the seismic data fold provided by the two year 70 km spaced EarthScope USArray sampling is sub-optimal.

We explore the physical properties gradient across the LAB as resulting from asthenospheric flow under the leading edge of a lithosphere that thickens to the east of the AMT. This flow is primarily driven by the drift of the North American plates as it has translated to the southwest at ∼2 cm/yr (Gripp and Gordon, 2002). At the leading edge of the thickening lithosphere, this flow may thermally ablate the base of the lithosphere to increase the thermal gradient at the base of the lithosphere (Till et al., 2010; Zaranek et al., 2002) (Fig. 5). However, this flow controlled thermal ablation effect is predicted to only slightly decrease the width between the 1300–1000° isotherms from 50 to 45 km assuming reasonable viscosity parameters (Zaranek, 2005). However, an additional flow effect that could increase the shear velocity decrement at the lithospheric base would be due to increased shear deformation where the mantle flow descends beneath the thickening lithosphere. This increased shear deformation would enhance the strength of the olivine fabric (Ribe, 1989) and hence the azimuthal anisotropy strength. We interpret the increase in azimuthal anisotropy strength to the east of the AMT as due to this effect (Figs. 3(e), 4(c), Supp. Fig. 3). While it is true that mantle channel flow beneath a uniform lithosphere is predicted to saturate the azimuthal anisotropy fabric strength (Kaminski and Ribe, 2002), inspection of the apparent shear wave splitting parameters that sample within our image volume (Yang et al., in press) shows that the splitting parameters are variable (Supp. Fig. 5) and hence saturation of the azimuthal anisotropic fabric due to plate shear does not seem true. To summarize, in a region of thickening lithosphere with mantle underflow, the combination of an increased basal thermal gradient and an increase in the azimuthal anisotropy strength, could produce a sufficiently sharp shear velocity gradient to produce a small amplitude Sp arrival.

To test this proposition, synthetic seismograms were calculated for an incident S-wave at 75° epicentral distance for a specified shear velocity decrement with different velocity gradient widths. To translate the 1000–1300 °C basal thermal gradient to its corresponding shear velocity decrement, a $dV_S/dT$ scaling of 1.3% per 100 °C at 200 km depth is used (Cammarano et al., 2003). This predicts a 3.9% shear velocity decrement across the basal thermal gradient. By comparison, the Yuan and Romanowicz (2010) tomogram images a mean shear velocity decrement at 190–260 km depth from 4.80 km/s to 4.62 km/s, which is a 3.8% decrement

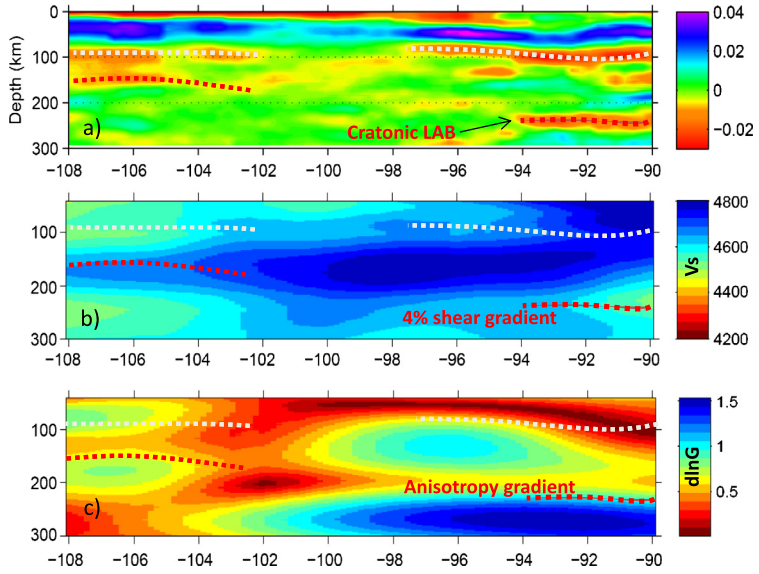


**Fig. 4.** E–W sections at 42°N. (a) Sp. (b) Isotropic shear velocity. (c) Azimuthal anisotropy strength ($d \ln G$). Note the correspondence between the east of AMT LAB arrival at 240 km depth (a), the 4% negative shear velocity gradient between 4800 and 4620 m/s (b), and the increase in the azimuthal anisotropy strength (c). The azimuthal fast-axis anisotropy direction is near the North American absolute plate direction of N50°E. Given that the majority of our S-waves arrive perpendicular to the fast anisotropic axis (i.e., along the slow axis) (Supp. Fig. 4), the anisotropy gradient will be dominantly sampled as a negative velocity gradient. The net effect of the isotropic and anisotropy gradients is modeled as an effective 6% shear decrement over a 45 km gradient width (Fig. 6). Note that the lateral resolution of the Sp image (110 km) and the velocity slices (400 km) are quite different and hence an exact correspondence with the cratonic LAB is not expected.

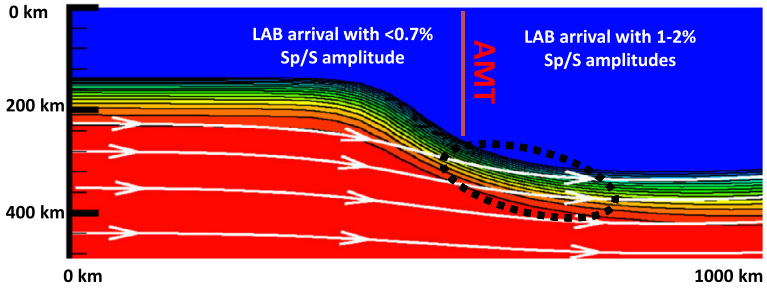


**Fig. 5.** Thick lithospheric root translating through fluid at 3 cm/yr from Zaranek (2005). The thermal field is contoured at 90 °C increments and the flow streamlines are shown. This model predicts that the flow under the cratonic root will only slightly reduce the width of the 1000–1300 °C isotherms outlined by the black dotted oval. However, the increased shear strain rate within the oval region will strengthen the olivine lattice preferred orientation and hence the velocity anisotropy. Both of these flow effects will increase the Sp negative velocity gradient conversion coefficient. This model is used to interpret the LAB arrival to the east of the upper American Midwest mantle transition (AMT).

(Fig. 4(b), Supp. Figs. 3, 4). However, the 70 km wide shear velocity gradient imaged by Yuan and Romanowicz (2010) is too wide to produce an observable Sp conversion (Rychert et al., 2007). Of course, in comparing our Sp images with the Yuan and Romanowicz (2010) model, one should bear in mind that the Yuan and Romanowicz (2010) models have a vertical resolution scale length of 30 km and a lateral resolution scale length for isotropic and anisotropic structure of 200 km and 500 km respectively (Yuan et al., 2011).

To reduce the width of the negative velocity gradient at the base of the lithosphere, we assess how a layer of enhanced azimuthal anisotropy at the base of the lithosphere (Fig. 4(e), Supp. Figs. 3, 4) could augment the isotropic shear velocity decrement across the LAB. First order to this analysis is the observation that 80% of our earthquakes are clustered around the slow azimuthal anisotropy axis in the asthenosphere as constrained by Yuan and Romanowicz (2010) (Supp. Fig. 6). Thus, when the receiver functions are averaged in the image domain, the net velocity effect will be a shear velocity decrement. Based on the increase in azimuthal anisotropy strength at the base of the lithosphere (Figs. 3(e), 4(c), Supp. Figs. 3, 4), an azimuthally averaged 2% shear velocity decrement is assumed. Given that high shear stresses are predicted where the down-sloping lithospheric base flattens out (Zaranek, 2005), we assume that the thermal and anisotropic velocity gradients are spatially correlated to produce a total shear velocity decrement of 6%.

To find a linear velocity gradient width that best fits our observations, a set of elastic synthetic seismograms (Park, 1996) were calculated (Fig. 6). The synthetic source function was a trapezoid with a 6 s upper frequency corner. This analysis is performed to fit the amplitude and approximate pulse-width of the cratonic LAB arrivals that is governed by the shear velocity decrement and velocity gradient width. Given the thermal and anisotropic velocity effects discussed above, a 6% shear velocity decrement is distributed over linear velocity gradient widths of 30, 45, and 60 km. The 60 km gradient is too wide to produce an Sp arrival and is therefore discounted. Whereas, the 30 and 45 km gradient models produce 1–2% amplitude arrivals with 35–45 km wide pulses that match the Sp observations to the east of the AMT (Figs. 2(a)–(d), 3(a)–(b)).

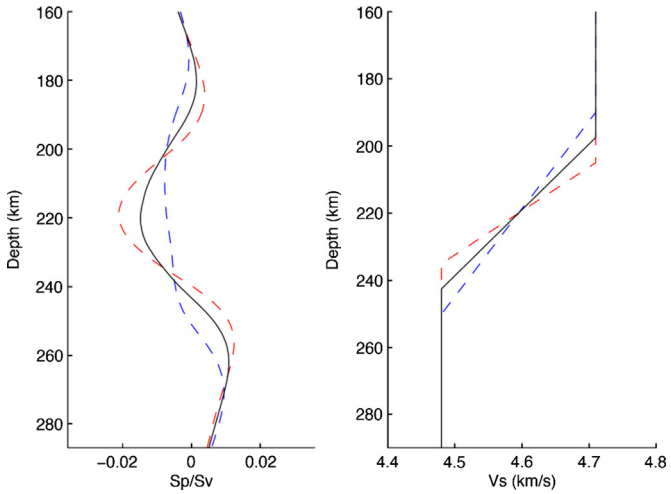


**Fig. 6.** Sp receiver function response for a 6% shear velocity decrement for color coded 30, 45, 60 km linear velocity gradient thicknesses. (a) Sp P-component receiver function for 75° delta incident SV wave band-pass filtered at 30–6 s. (b) Linear velocity gradients at LAB. The 45 km gradient predicts a 1.5% Sp/Sv amplitude consistent with the amplitudes and pulse-width for LAB arrivals imaged east of the AMT (Figs. 2(a)–(d), 3(a)–(b)).

### 3.2. Mid-lithospheric discontinuity

While the deep LAB arrival is our primary finding, we would be remiss to not address the large negative velocity gradient arrivals at 70–110 km depth in our image (Figs. 2(a)–(d), 3(a)–(b)). This 2–3% Sp/S amplitude arrival is higher in amplitude with respect to the LAB. This MLD arrival shows 30 km of depth variation and is sometimes imaged as two shingled arrivals. Interestingly, the amplitude of our MLD signals dims to near zero within the Trans-Hudson orogeny and Yavapai provinces (Figs. 2(a)–(d), 3(a), (b)). Comparison of our MLD structure with the Yuan and Romanowicz (2010) velocity layering does not find a corresponding negative isotropic velocity gradient (Fig. 4, Supp. Figs. 3, 4). Therefore, our American upper Midwest MLD arrivals are not consistent with anisotropic velocity modulation of Sp conversions to make a negative velocity gradient as proposed for the Canadian shield (Yuan and Romanowicz, 2010).

## 4. Discussion

### 4.1. Cratonic LAB

Previous Sp imaging in thick lithosphere regions has found negative velocity gradients interpreted as the LAB at 220 km under the Baltic shield (Sacks et al., 1979), at 172 km under eastern Montana, USA (Baumgardt and Alexander, 1984), and at ∼200 km beneath the Canadian Shield (Miller and Eaton, 2010). A tangential Ps arrival at 170–200 km has also been observed beneath the Slave craton (Snyder, 2008). For the North American continent, Yuan and Romanowicz (2010) produced an LAB depth map based on vertical variations in azimuthal anisotropy to report an LAB at 180–240 km depth beneath the upper American Midwest with lateral resolution of about 200 km.

Equally important to LAB arrival imaging is the absence of observable Sp LAB arrivals beneath much of the thick lithosphere regions of North America (Abt et al., 2010; Kumar et al., 2012), the Kapaaval craton (Jasbinsek et al., 2010; Savage and Silver, 2008), the Australian continent (Ford et al., 2010), and globally (Rychert et al., 2010). In thick lithosphere areas, the non-observations of an Sp LAB arrival are important because two interpretations exist: either the shear velocity gradients are too small to convert significant Sp energy, or the seismic data sampling fold is insufficient.

For a cratonic root translating through the mantle, an acceleration of the mantle as it flows beneath leading edge of the thickening lithosphere only predicts small reduction in the width of the basal thermal gradient from 50 to 45 km, given reasonable thermally-dependent rheology (Zaranek et al., 2002). This velocity gradient width using a 3.9% shear velocity decrement associated with the basal lithospheric temperature gradient is insufficient to produce our 1–2% Sp LAB arrival amplitudes. Hence, the seismic velocity effects of enhanced shear strain rates where the mantle flows under the thickened lithosphere were considered. This increased shear strain rate, hence increased olivine lattice preferred orientation, would be seismically sensed as an increased shear wave azimuthal anisotropy strength (Kaminski and Ribe, 2002; Ribe, 1989).

Convective flow solutions that simultaneously fit the World Stress Map, plate velocities, and the poloidal/torrodial ratio find that the stress traction field at 100 km depth beneath the upper American Midwest is directed at N70°E (Ghosh et al., 2013; Ghosh et al., 2013). This traction field is dominantly produced by mantle flow toward N70°E to underflow the region of thickened lithosphere. Noteworthy is that this local stress traction field is nearly perpendicular to the AMT consistent with mantle underflow of the thickened lithosphere. The southwestward drift of the North American plate since the opening of the North Atlantic means the mantle flow under the thickened lithosphere has been occurring for 90 Ma (Kreemer et al., 2003). Thus, we can assume that the thermal boundary layer ablation and olivine LPO evolution are in a steady dynamical state (Kaminski and Ribe, 2002).

Azimuthal anisotropy, as sampled by SKS shear wave anisotropy, has been used to assess the direction of mantle flow around lithospheric thickness undulations (Assumpcao et al., 2006; Behn et al., 2004; Conrad et al., 2007; Fouch et al., 2000; Refayee et al., 2013) and the strength of basal tractions beneath the Canadian Shield (Bokelmann et al., 2000). In the southern Midwest region, SKS anisotropy analysis finds coherent changes in fast axis orientation that could relate to mantle flow beneath an undulating lithosphere (Refayee et al., 2013). In the upper Midwest region, a shear wave splitting analysis performed by Yang et al. (in press) finds variable patterns of apparent fast axis anisotropy (Supp. Fig. 5).

### 4.2. Mid-lithospheric discontinuity comparison

Comparison of our results with Sp results from the analysis of long operating stations finds good agreement for the MLD arrival depths. National Seismic Network stations and a Canadian Digital Seismic Network station (Fig. 1) have Sp negative velocity gradient arrivals reported at 88 (CCM), 101 (FVM), 77 (SLM), 69 (CBKS), 94 (EYNM), 79 (ISCO), 59 (JWFS), and 101 (ULM) km depth (Abt et al., 2010). The mean MLD depth from these observations is 83 km. Our corresponding MLD depths under these stations are in the 70–110 km range with a mean depth of 87 km and hence we conclude that our MLD depths are consistent with these prior findings.

Yet, for the stations east of the AMT, the Abt et al. (2010) analysis did not find a deep LAB arrival. To explain this difference, we note two primary differences in our processing. First, single station receiver function stacks are averages over a wide range of incident S-wave azimuths and ray parameters. This means that at 200 km depth a single station stack is averaging data over an annulus with a 100–250 km radius from the station (Yuan et al., 2006b). This very large sampling area can produce stack incoherence if there are significant structural variations within the sampling annulus. Second, our deconvolution method is quite different from Abt et al. (2010) method. Hence, our ability to image a deep weak Sp LAB arrival beneath the upper Midwest is because: (1) the 400 seismic stations EarthScope USArray data permits a more accurate estimation of the incident source wavelet,

and hence higher quality receiver functions; (2) USArray data permits three-dimensional imaging to be performed rather than analyzing single station stack averages. Within our sampling area, two other Sp RF images based on USArray data find a negative velocity gradient MLD arrival at 75–95 km depth (Kumar et al., 2012), and at 80–110 km (Levander and Miller, 2012).

### 4.3. Mid-lithospheric discontinuity origins

Models to explain the origin of cratonic MLD signals are: (1) non-eclogtized oceanic crust entombed during the accretion process (Bostock et al., 2010); (2) grain-boundary sliding anelasticity enabled by hydration effects (Karato, 2012); (3) aluminous-orthopyroxene water solubility melt effect (Mierdel et al., 2007); (4) the accumulation of a layer of low-velocity minerals due to the infiltration of $CO_2$/$H_2O$/K-rich magmas which crystallize at 2–3 GPa (60–90 km) over Ga time-scales (McKenzie, 1989). We rule out model (1) because our MLD layer is too extensive and has little structural dip. Model (2) is possible, but at present the model is speculative and no data with respect to lithospheric mantle hydration exists in this region. Model (3) predicts a water solubility minimum for a cratonic geotherm that is too deep (150 km) with respect to our observations.

Thus, we conclude that a metasomatic layer (model 4) is the most plausible interpretation of our MLD signals, as other work in cratonic areas has concluded (Chen et al., 2009; Savage and Silver, 2008; Wolbern et al., 2012). This conclusion is consistent with the 540 Ma REE-rich Elk-Creek carbonatite intrusion in SE Nebraska with a mantle $Sr_{87}/Sr_{86}$ ratio of 0.7027 (Farmer, 2013) being derived via re-melting of a pre-existing metasomatic mineral rich layer (Pilet et al., 2008). This conclusion is also consistent with the petrogenesis of carbonatite intrusions in the Black Hills, South Dakota, and in eastern Montana (Fig. 1) (Duke, 2009).

## 5. Conclusions

Our Sp LAB structure and amplitudes observed to the east of the AMT are consistent with a 6% shear velocity decrement over a 45 km wide linear gradient. This shear velocity decrement is consistent with the combination of the anelastic thermal velocity effects over a 1000–1300 °C basal thermal gradient along with the fact that 80% of our incident S-waves sample the slow azimuthal anisotropy axis in the asthenospheric layer. The mantle down-flow along the down-sloping lithosphere will produce high shear strains consistent with the observation of high azimuthal anisotropy to the east of the AMT. Given that our seismic velocity gradients can sense the basal temperature interval and olivine LPO development, future work in areas of deepening lithosphere can help constrain the viscosity gradients which couple the rigid lithospheric blocks to the underlying buoyancy-driven mantle flow. Our MLD signals are interpreted as a metasomatic layer with high modal concentration of low-velocity minerals that have been re-melted to make the carbonatite intrusions within this area. The general absence of MLD signals beneath the Trans-Hudson Proterozoic mobile belt likely relates to the mode of construction of the Trans-Hudson province versus the Superior and Yavapai provinces.

## Appendix A. Supplementary material

Supplementary material related to this article can be found online at http://dx.doi.org/10.1016/j.epsl.2013.11.018.

## References


Abt, D., Fischer, K., French, S.W., Ford, H., Yuan, H.Y., Romanowicz, B., 2010. North American lithospheric discontinuity structure imaged by Ps and Sp receiver functions. J. Geophys. Res. 115. http://dx.doi.org/10.1029/2009jb006914.

Assumpcao, M., Heintz, M., Vauchez, A., Silva, M.E., 2006. Upper mantle anisotropy in SE and Central Brazil from SKS splitting: Evidence of asthenospheric flow around a cratonic keel. Earth Planet. Sci. Lett. 250, 224–240. http://dx.doi.org/10.1016/j.epsl.2006.07.038.

Baumgardt, D., Alexander, S., 1984. Structure of the mantle beneath Montana LASA from analysis of long-period, mode-converted phases. Bull. Seismol. Soc. Am. 74, 1683–1702.

Behn, M.D., Conrad, C.P., Silver, P.G., 2004. Detection of upper mantle flow associated with the African Superplume. Earth Planet. Sci. Lett. 224, 259–274.

Bokelmann, G.H.R., Silver, P.G., Rumpker, G., 2000. Mantle variation within the Canadian Shield: Travel times from the portable broadband Archean–Proterozoic Transect 1989. J. Geophys. Res. 105, 579–605.

Bostock, M., 2004. Greens functions, source signatures, and the normalization of teleseismic wave fields. J. Geophys. Res. 109. http://dx.doi.org/10.1029/2003jb002783.

Bostock, M.G., Eaton, D.W., Snyder, D., 2010. Teleseismic studies of the Canadian landmass: Lithoprobe and its legacy. Can. J. Earth Sci. 47, 445–906. http://dx.doi.org/10.1139/e09-040.

Cammarano, F., Goes, S., Vacher, P., Giardini, D., 2003. Inferring upper-mantle temperatures from seismic velocities. Phys. Earth Planet. Inter. 138, 197–222.

Chen, C.-W., Rondenay, S., Evans, R., Snyder, D., 2009. Geophysical detection of relict metasomatism from an Archean (approximately 3.5 Ga) subduction zone. Science 326, 1089–1180. http://dx.doi.org/10.1126/science.1178477.

Conrad, C.P., Behn, M.D., Silver, P.G., 2007. Global mantle flow and the development of seismic anisotropy: Differences between the oceanic and continental upper mantle. J. Geophys. Res. 112. http://dx.doi.org/10.1029/2006JB004608.

Cooper, C.M., Conrad, C.P., 2009. Does the mantle control the maximum thickness of cratons?. Lithos 1, 67–72. http://dx.doi.org/10.1130/L40.1.

Dueker, K.G., Sheehan, A.F., 1997. Mantle discontinuity structure from midpoint stacks of converted P and S waves across the Yellowstone hotspot track. J. Geophys. Res. 102, 8313–8327.

Duke, G.I., 2009. Black Hills–Alberta carbonatite–kimberlite linear trend: Slab edge at depth?. Tectonophysics 464, 186–380. http://dx.doi.org/10.1016/j.tecto.2008.09.034.

Farmer, L., 2013. Geochemical and isotropic constraints on the age and origin of the Elk Creek carbonatite complex, SE Nebraska. In: Geo. Soc. Am. Rocky Mt. Ann. Meeting.

Farra, V., Vinnik, L., 2000. Upper mantle stratification by P and S receiver functions. Geophys. J. Int. 141, 699–712.

Ford, H., Fischer, K., Abt, D., Rychert, C., 2010. The lithosphere–asthenosphere boundary and cratonic lithospheric layering beneath Australia from Sp wave imaging. Earth Planet. Sci. Lett.. http://dx.doi.org/10.1016/j.epsl.2010.10.007.

Forsyth, D., Uyeda, S., 1975. On the relative importance of the driving forces of plate motion. Geophys. J. R. Astron. Soc. 43, 163–200.

Fouch, M.J., Fischer, K.M., Parmentier, E.M., Wysession, M.E., Clarke, T.J., 2000. Shear wave splitting, continental keels, and patterns of mantle flow. J. Geophys. Res. 105, 6255–6275.

Ghosh, A., Holt, W.E., 2012. Plate motions and stresses from global dynamic models. Science 335, 838–843. http://dx.doi.org/10.1126/science.1214209.

Ghosh, A., Holt, W.E., Wen, L., 2013. Predicting the lithospheric stress field and plate motions by joint modeling of lithosphere and mantle dynamics. J. Geophys. Res. 118, 346–368. http://dx.doi.org/10.1029/2012JB009516.

Ghosh, A., Becker, T., Humpreys, E., 2013. Dynamics of North American continent. Geophys. J. Int. 194, 651–669. http://dx.doi.org/10.1093/gji/ggt151.

Gripp, A.E., Gordon, R.G., 2002. Young tracks of hotspots and current plate velocities. Geophys. J. Int. 150, 321–361.

Hansen, S., Dueker, K., 2009. P- and S-wave receiver function images of crustal imbrication beneath the Cheyenne Belt in southeast Wyoming. Bull. Seismol. Soc. Am.. http://dx.doi.org/10.1785/0120080168.

Jasbinsek, J., Dueker, K., Hansen, S., 2010. Characterizing the 410 km discontinuity low velocity layer beneath the LA RISTRA array in the North American Southwest. Geochem. Geophys. Geosyst. 11. http://dx.doi.org/10.1029/2009GC002836.

Julià, J., 2007. Constraining velocity and density contrasts across the crust–mantle boundary with receiver function amplitudes. Geophys. J. Int. 171, 286–587. http://dx.doi.org/10.1111/j.1365-2966.2007.03502.x.

Kaminski, E., Ribe, N.M., 2002. Timescales for the evolution of seismic anisotropy in mantle flow. Geochem. Geophys. Geosyst. 3.

Karato, S.-i., 2012. On the origin of the asthenosphere. Earth Planet. Sci. Lett. 321–322. http://dx.doi.org/10.1016/j.epsl.2012.01.001.

Kolmogorov, A., 1939. Sur l'interpolation et l'extrapolation des suites stationnaries. C. R. Acad. Sci. 208, 2043–2045.

Kreemer, C., Holt, W.E., Haines, A.J., 2003. An integrated global model of present-day plate motions and plate boundary deformation. Geophys. J. Int. 154, 8–34. http://dx.doi.org/10.1046/j.1365-246X.2003.01917.x.

Kumar, P., Yuan, X., Kind, R., Mechie, J., 2012. The lithosphere–asthenosphere boundary observed with USArray receiver functions. Solid Earth 4. http://dx.doi.org/10.5194/sed-4-1-2012.

Langston, C.A., 1977. Corvallis, Oregon, crustal and upper mantle receiver structure from teleseismic P and S waves. Bull. Seismol. Soc. Am. 67, 713–724.

Lebedev, S., Boonen, J., Trampert, J., Snyder, D.B., Francis, D., 2009. Seismic structure of Precambrian lithosphere; new constraints from broad-band surface wave dispersion. Lithos 109, 96–111. http://dx.doi.org/10.1016/j.lithos.2008.06.010.

Levander, A., Miller, M.S., 2012. Evolutionary aspects of lithosphere discontinuity structure in the western U.S. Geochem. Geophys. Geosyst. 13, Q0AK07. http://dx.doi.org/10.1029/2012GC004056.

McKenzie, D.M., 1989. Some Remarks on the movement of small melt fractions in the mantle. Earth Planet. Sci. Lett. 95, 53–72.

Mercier, J.P., Bostock, M., Baig, A.M., 2006. Improved Green's functions for passive source structural studies. Geophysics 22.

Mierdel, K., Keppler, H., Smyth, J., Langenhorst, F., 2007. Water solubility in aluminous orthopyroxene and the origin of Earth's asthenosphere. Science 315, 364–372. http://dx.doi.org/10.1126/science.1135422.

Miller, M.S., Eaton, D.W., 2010. Formation of cratonic mantle keels by arc accretion: Evidence from S receiver functions. Geophys. Res. Lett. 37. http://dx.doi.org/10.1029/2010gl044366.

Park, J., 1996. Surface waves in layered anisotropic structures. Geophys. J. Int. 126, 173–184.

Pedersen, H.A., Fishwick, S., Snyder, D.B., Francis, D., 2009. A comparison of cratonic roots through consistent analysis of seismic surface waves. Lithos 109, 81–95. http://dx.doi.org/10.1016/j.lithos.2008.09.016.

Pilet, S., Baker, M., Stolper, E., 2008. Metasomatized lithosphere and the origin of alkaline lavas. Science 320, 916–925. http://dx.doi.org/10.1126/science.1156563.

Refayee, H.A., Yang, B.B., Liu, K.H., Gao, S.S., 2013. Mantle flow and lithosphere–asthenosphere coupling beneath the southwestern edge of the North American craton: Constraints from shear-wave splitting measurements. J. Geophys. Res.. http://dx.doi.org/10.1016/j.epsl.2013.01.031.

Ribe, N.M., 1989. Seismic anisotropy and mantle flow. J. Geophys. Res. 94, 4213–4223.

Rychert, C., Fischer, K., Rondenay, S., 2005. A sharp lithosphere–asthenosphere boundary imaged beneath eastern North America. Nature 436, 542–547. http://dx.doi.org/10.1038/nature03904.

Rychert, K., Rondenay, S., Fischer, K., 2007. P-to-S and S-to-P imaging of a sharp lithosphere–asthenosphere boundary beneath eastern North America. J. Geophys. Res.. http://dx.doi.org/10.1029/2006jb004619.

Rychert, K., Shearer, P., Fischer, K., 2010. Scattered wave imaging of the lithosphere–asthenosphere boundary. Lithos 120. http://dx.doi.org/10.1016/j.lithos.2009.12.006.

Sacks, I., Snoke, J., Husbeye, E., 1979. Lithospheric thickness beneath the Baltic Shield. Tectonophysics 56, 101–110.

Savage, B., Silver, P.G., 2008. Evidence for a compositional boundary within the lithospheric mantle beneath the Kalahari craton from S receiver functions. Earth Planet. Sci. Lett. 272, 600–609. http://dx.doi.org/10.1016/j.epsl.2008.05.026.

Shen, W., Ritzwoller, M.H., Schulte-Pelkum, V., 2013. A 3-D model of the crust and uppermost mantle beneath the Central and Western US by joint inversion of receiver functions and surface wave dispersion. J. Geophys. Res. 118, 262–276. http://dx.doi.org/10.1029/2012jb009602.

Sleep, N.H., 2011. Seismically observable features of mature stagnant-lid convection at the base of the lithosphere: Some scaling relationships. Geochem. Geophys. Geosyst. 12. http://dx.doi.org/10.1029/2011gc003760.

Snyder, D.B., 2008. Stacked uppermost mantle layers within the Slave craton of NW Canada as defined by anisotropic seismic discontinuities. Tectonics 27, TC4006. http://dx.doi.org/10.1029/2007TC002132.

Till, C.B., Elkins-Tanton, L.T., Fischer, K.M., 2010. A mechanism for low-extent melts at the lithosphere–asthenosphere boundary. Geochem. Geophys. Geosyst. 11. http://dx.doi.org/10.1029/2010gc003234.

Vinnik, L.P., 1977. Detection of waves converted from P to SV in the mantle. Phys. Earth Planet. Inter. 15, 39–45.

Wolbern, I., Ruempker, G., Link, K., Sodoudi, F., 2012. Melt infiltration of the lower lithosphere beneath the Tanzania craton and the Albertine rift inferred from S receiver functions. Geochem. Geophys. Geosyst. 13. http://dx.doi.org/10.1029/2012gc004167.

Yang, B., Gao, S., Liu, K., Elsheikh, A., Lemnifi, A., Rafayee, A., Yu, Y., in press. Seismic anisotropy and mantle beneath the northern Great Plains of North America. J. Geophys. Res.

Yuan, H., Romanowicz, B., 2010. Depth dependent azimuthal anisotropy in the western US upper mantle. Earth Planet. Sci. Lett. 300, 385–779. http://dx.doi.org/10.1016/j.epsl.2010.10.020.

Yuan, H.Y., Romanowicz, B., 2010. Lithospheric layering in the North American craton. Nature 466, 1063–1071. http://dx.doi.org/10.1038/nature09332.

Yuan, H., Romanowicz, B., Fischer, K.M., Abt, D., 2011. 3-D shear wave radially and azimuthally anisotropic velocity model of the North American upper mantle. Geophys. J. Int. 184, 1237–1260. http://dx.doi.org/10.1111/j.1365-246X.2010.04901.x.

Yuan, X., Kind, R., Li, X., Wang, R., 2006a. The S receiver functions: synthetics and data example. Geophys. J. Int. 165, 555–1119. http://dx.doi.org/10.1111/j.1365-246X.2006.02885.x.

Yuan, X., Kind, R., Li, X., 2006b. The S receiver functions: synthetics and data example. Geophys. J. Int.. http://dx.doi.org/10.1111/j.1365-246X.2006.02885.x.

Zaranek, S., 2005. Roles of convection in the evolution of planetary interiors and terrestrial lithospheres. PhD thesis.

Zaranek, S.E., Parmentier, E.M., Fischer, K.M., 2002. Basal drag and the erosion of subcratonic lithosphere. EOS Trans. Am. Geophys. Union 83, 1.